TU Delft

Delft University of Technology

Document Version
Final published version

Licence
CC BY

Citation (APA)
Kariminejad, M. M., Sharifi, M. A., Amiri-Simkooei, A., & Mostafavi, M. A. (2026). Stochastic and functional modeling of RSSI measurements for accurate distance estimation in bluetooth low energy–based indoor positioning. *Measurement: Journal of the International Measurement Confederation*, *289*, Article 122582. https://doi.org/10.1016/j.measurement.2026.122582

Important note
To cite this publication, please use the final published version (if applicable).
Please check the document version above.

Copyright
In case the licence states “Dutch Copyright Act (Article 25fa)”, this publication was made available Green Open Access via the TU Delft Institutional Repository pursuant to Dutch Copyright Act (Article 25fa, the Taverne amendment). This provision does not affect copyright ownership.
Unless copyright is transferred by contract or statute, it remains with the copyright holder.

Sharing and reuse
Other than for strictly personal use, it is not permitted to download, forward or distribute the text or part of it, without the consent of the author(s) and/or copyright holder(s), unless the work is under an open content license such as Creative Commons.

Takedown policy
Please contact us and provide details if you believe this document breaches copyrights.
We will remove access to the work immediately and investigate your claim.

This work is downloaded from Delft University of Technology.

Measurement 289 (2026) 122582

Contents lists available at ScienceDirect

Measurement

journal homepage: www.elsevier.com/locate/measurement

Stochastic and functional modeling of RSSI measurements for accurate distance estimation in bluetooth low energy–based indoor positioning

Mohammad Mahdi Kariminejad [a], Mohammad Ali Sharifi [a], Alireza Amiri-Simkooei [b,*], Mir Abolfazl Mostafavi [c]

[a] School of Surveying and Geospatial Engineering, College of Engineering, University of Tehran, Tehran, Iran
[b] Department of Control and Operations, Faculty of Aerospace Engineering, Delft University of Technology, Delft, Netherlands
[c] Department of Geomatic Sciences, Faculty of Forestry Geography and Geomatics, Laval University Quebec City, Quebec, Canada

ARTICLE INFO

Keywords:
Bluetooth Low Energy (BLE)
Received Signal Strength Indicator (RSSI)
RSSI-distance modeling
Colored noise
Least Squares Variance Component Estimation (LS-VCE)
Maximum Likelihood Estimation (MLE)

ABSTRACT

This study presents a comprehensive mathematical framework for modeling Bluetooth Low Energy (BLE) beacon Received Signal Strength Indicator (RSSI) measurements to improve the estimation of RSSI-distance model parameters through the integration of stochastic and functional modeling. Although such approaches are well established in geodesy, they have been only sparsely applied to indoor positioning, particularly for characterizing RSSI dependencies arising from multipath propagation. Experiments were conducted using two types of BLE beacons in a controlled static outdoor environment to isolate signal behavior and facilitate reliable RSSI–distance modeling. Outliers were mitigated using a median filter based on local neighborhood comparisons. Stochastic modeling was then performed using the autocorrelation function (ACF) and partial autocorrelation function (PACF), revealing that RSSI noise exhibits short-memory, time-correlated behavior that is well represented by a second-order autoregressive AR(2) model. Measurement weights were estimated using Least Squares Variance Component Estimation (LS-VCE), followed by functional modeling for the estimation of environmental and beacon transmit-power parameters together with their uncertainties. The estimated candidate AR models were further compared using their maximized log-likelihood values, which confirmed that the AR(2) model provides the most appropriate representation of the RSSI noise process. The reconstructed RSSI achieved root mean square errors (RMSEs) of 1.12 dBm and 0.50 dBm for the IT002 and IT008 beacons, respectively, at a distance of 1 m, increasing to 2.19 dBm and 2.40 dBm at 10 m. These errors correspond to relative distance uncertainties of approximately 6–13% at 1 m and 15–25% at 10 m, demonstrating the effectiveness of the proposed framework for accurate RSSI modeling and parameter estimation.

1. Introduction

Indoor positioning systems (IPS) comprise a broad range of technologies designed to provide accurate location information in environments where Global Navigation Satellite System (GNSS) signals are unavailable or severely degraded. The selection of an appropriate positioning technology depends on the specific requirements of the application, including accuracy, infrastructure availability, energy consumption, deployment cost, and environmental conditions [1]. Among the available solutions, radio frequency (RF)-based technologies have attracted considerable attention because of their scalability, low deployment cost, and compatibility with existing wireless infrastructures.

Common RF-based IPS technologies include Bluetooth Low Energy (BLE) [2,3], Wireless Fidelity (Wi-Fi) [4,5], ZigBee [6], Radio Frequency Identification (RFID) [7], and Ultra-Wideband (UWB) [8]. Considerable research has been devoted to developing mathematical models, signal-processing algorithms, and sensor-fusion techniques to improve the positioning accuracy and robustness of these technologies. Each RF technology possesses distinct characteristics that influence its suitability for specific indoor positioning applications. BLE has emerged as a popular solution because of its low power consumption, low hardware cost, and ease of deployment [9]. Wi-Fi benefits from widespread infrastructure availability, making it attractive for large-scale positioning systems [10], although its performance is often degraded by multipath propagation and signal fluctuations [11]. ZigBee is designed for low-power and low-data-rate wireless communication and commonly relies on Received Signal Strength Indicator (RSSI) measurements for localization [12]; however, its positioning performance can be affected by limited communication range and

* Corresponding author.
E-mail address: a.amirisimkooei@tudelft.nl (A. Amiri-Simkooei).

https://doi.org/10.1016/j.measurement.2026.122582
Received 31 March 2026; Received in revised form 11 June 2026; Accepted 13 July 2026
Available online 21 July 2026
0263-2241/© 2026 The Authors. Published by Elsevier Ltd. This is an open access article under the CC BY license (http://creativecommons.org/licenses/by/4.0/).

interference [13]. RFID is particularly effective for asset tracking and inventory management applications, where the presence of tagged objects can be reliably detected [14]. In contrast, UWB offers superior ranging accuracy due to its large signal bandwidth and fine temporal resolution, and is frequently combined with advanced filtering and fusion methods to further enhance positioning performance [15,16]. Given these differences, selecting an appropriate RF technology requires careful consideration of the application requirements, environmental conditions, infrastructure constraints, and desired positioning accuracy.

Among these technologies, BLE has emerged as one of the most widely adopted solutions for indoor positioning because of its efficiency, versatility, and extensive integration into consumer and industrial devices. BLE-based systems support a wide range of applications, including asset tracking, indoor navigation, proximity services, smart buildings, and location-based services [17]. The rapid evolution of Bluetooth technology has further strengthened its role in indoor positioning. The introduction of Apple's iBeacon protocol in 2013 and Google's Eddystone protocol in 2015 established standardized beacon-based localization frameworks. Subsequent Bluetooth releases, including version 5.0 in 2016 and version 5.1 in 2019, introduced extended communication range, higher data rates, and direction-finding capabilities, enabling increasingly accurate localization solutions. Bluetooth 5.2, released in 2020, further enhanced the Bluetooth Low Energy (BLE) ecosystem through improved power efficiency, more reliable communication, and support for advanced features such as LE Isochronous Channels, which facilitate synchronized data transmission. More recently, Bluetooth 5.3 and Bluetooth 5.4 have focused on increasing network efficiency, reducing latency and power consumption, and improving support for large-scale deployments of connected devices. These advancements, together with the direction-finding capabilities introduced in Bluetooth 5.1 based on Angle of Arrival (AoA) and Angle of Departure (AoD) techniques, have significantly improved the scalability, robustness, and positioning accuracy of BLE-based indoor localization systems, making Bluetooth one of the most widely adopted technologies for indoor positioning applications.

Despite these advantages, BLE-based indoor positioning systems face several fundamental challenges. The most widely used measurement observable, the RSSI, follows a logarithmic distance-dependent attenuation model and is highly sensitive to environmental conditions [18]. Signal propagation is affected by structural obstacles, shadowing, multipath propagation, interference, and hardware limitations [19,20]. Furthermore, receiver motion and dynamic environmental changes introduce rapid RSSI fluctuations. Consequently, RSSI measurements often exhibit substantial variability, making reliable distance estimation difficult [21]. These effects complicate the development of accurate RSSI–distance models and limit positioning performance.

To mitigate these limitations, numerous studies have investigated signal-processing, filtering, machine learning, and sensor-fusion techniques for BLE-based indoor positioning. Early studies established the foundations of Bluetooth localization. Hossain and Soh [22] examined the effects of RSSI, Link Quality, and transmit power on localization performance. Pei et al. [23] introduced a stochastic framework based on Weibull-distributed RSSI measurements and maximum likelihood estimation (MLE), while Subhan et al. [24] improved RSSI-based ranging using gradient filtering techniques.

Subsequent studies focused on improving RSSI modeling and positioning algorithms. Kajioka [25] investigated BLE beacon sensing characteristics, whereas Ji et al. [26] compared BLE and Wi-Fi measurements and highlighted the benefits of dense beacon deployment. Several researchers proposed filtering and optimization approaches to address RSSI fluctuations, including smoothing techniques [27], neural network optimization [28], particle filtering [29], Kalman filtering [30,31], iterative weighted K-nearest neighbors [32], and hybrid trilateration-fingerprinting approaches [33]. Additional investigations employed least-squares estimation and centroid-based localization models [34].

The integration of BLE with advanced estimation methods and complementary sensors subsequently became a major research direction. Kalman filtering was applied to improve RSSI measurements in practical deployments [35], while wavelet transforms and smoothing filters were investigated to increase positioning stability [36]. Multi-stage positioning frameworks combining propagation models, correction coefficients, trilateration, and filtering techniques were also proposed [37]. Sensor fusion approaches integrating BLE with inertial measurement units (IMUs) and pedestrian dead reckoning (PDR) demonstrated significant performance improvements [38–40]. Other studies explored machine-learning approaches [41], hybrid localization frameworks [42], lightweight fingerprinting techniques [19], and accessibility-oriented positioning systems [43,44].

Recent research has increasingly focused on deep learning, optimization, and hybrid positioning strategies. Particle swarm optimization (PSO) and related nature-inspired methods have been employed to improve localization accuracy [45,46]. Deep neural network (DNN)-based positioning frameworks have also been proposed [47]. Comprehensive surveys have classified Bluetooth localization techniques into six principal categories: proximity sensing, time difference of arrival (TDoA), trilateration, fingerprinting, AoA, and AoD [48,49]. More recently, RSSI-based fingerprinting approaches [50], signal propagation modeling techniques [51], and RSSI–AoA fusion frameworks [52] have further advanced BLE positioning capabilities.

Recent advances in measurement and sensing technologies have also contributed to RSSI processing and localization accuracy [53,54]. Various studies have applied Kalman filtering [55,56], neural network optimization, Monte Carlo simulation [57], and related mathematical methods [58] to smooth RSSI measurements and improve deterministic RSSI–distance modeling. However, despite these advances, the majority of existing studies focus primarily on the functional formulation of positioning models.

A critical limitation of the current literature is the insufficient treatment of the stochastic properties of RSSI measurements. While uncertainty analysis has recently received greater attention [59,60], RSSI observations are still commonly assumed to be independent [52,61–63]. In practice, severe multipath propagation, environmental dynamics, and hardware limitations generate temporally correlated observations characterized by colored-noise behavior. Neglecting these stochastic dependencies can lead to biased parameter estimation, unrealistic uncertainty assessments, and degraded positioning performance.

To address this research gap, this study proposes a comprehensive mathematical framework that jointly integrates stochastic and functional modeling of BLE RSSI measurements. The stochastic behavior of RSSI observations is first characterized using the autocorrelation function (ACF) and partial autocorrelation function (PACF), widely used tools for time-series and random-process analysis [64,65]. The resulting stochastic model is then used within a Least Squares Variance Component Estimation (LS-VCE) framework to estimate realistic measurement weights and covariance structures [66,67]. Subsequently, the functional RSSI–distance model is estimated using Best Linear Unbiased Estimation (BLUE), allowing simultaneous estimation of environmental and beacon parameters together with their uncertainties. Similar stochastic modeling principles have proven effective in Global Positioning System (GPS) uncertainty analysis [68], but have rarely been applied to BLE RSSI positioning.

The principal novelty of this work lies in moving beyond the conventional assumption of independent RSSI observations and establishing a unified stochastic–functional framework capable of representing both deterministic signal attenuation and stochastic measurement dependencies. By explicitly modeling temporal correlations, the proposed approach improves parameter estimation, uncertainty quantification, and positioning reliability in BLE-based indoor positioning systems.

Table 1 summarizes representative BLE positioning methods reported during the past decade and highlights the distinctive contribution of the proposed framework.

Table 1
A decade-long review of representative BLE indoor positioning methods.

Method	Year	Technique	Reference	Stochastic modeling	Accuracy
UKF/IW-KNN	2016	Weighted distance estimation	Peng et al. [32]	Partial	High
Graph optimization	2018	Trilateration + fingerprinting	Zuo et al. [33]	Partial	High
Nature-Inspired/DL	2022	Optimization-based positioning	Bencak et al. [46]; Koutris et al. [47]	Partial	High
PSO	2024	Optimization-based positioning	Assayag et al. [45]	Partial	High
Kalman filter	2025	RSSI–AoA data fusion	Fabris et al. [52]	Partial	Very high
This study	2026	Stochastic and functional modeling	Kariminejad et al. (this study)	Full	Very high

The remainder of this paper is organized as follows. Section 2 presents the proposed methodology, including stochastic and functional modeling procedures. Section 3 describes the experimental setup and case studies. Section 4 presents and discusses the results. Finally, Section 5 concludes the paper and outlines future research directions.

2. Methodology

This study proposes a comprehensive framework for modeling BLE RSSI measurements aimed at improving the accuracy and reliability of RSSI–distance parameter estimation. The methodology begins with outlier detection using a median filter to identify and mitigate impulsive noise and transient spikes in raw RSSI measurements, thereby providing a robust foundation for subsequent analysis. The core focus of this work is the stochastic modeling of RSSI measurements, which explicitly addresses the dependencies induced by strong multipath effects, particularly in indoor environments. By characterizing the time-correlated and short-memory behavior of RSSI noise through autocorrelation analysis and variance component estimation, this step enables the accurate construction of the cofactor matrix and corresponding measurement weights. Subsequently, functional modeling is employed to estimate the key parameters of the RSSI–distance model, including environmental factors and beacon transmit power, together with their associated uncertainties. This enables reliable reconstruction of RSSI values and derivation of distance estimates with quantified confidence. Collectively, these steps constitute a systematic methodological framework for preprocessing, characterizing, and modeling BLE RSSI measurements, specifically targeting the challenges posed by multipath-induced stochastic behavior. Finally, MLE criterion is applied to validate the proposed stochastic model by quantifying the agreement between the assumed noise characteristics and the observed RSSI measurements, see [69].

2.1. Outlier detection using the median filter

Outlier detection is a critical preprocessing step in RSSI-based positioning, as raw BLE measurements are often contaminated by impulsive disturbances caused by interference, hardware instability, and short-term multipath fading. Such anomalies can severely bias subsequent stochastic and functional modeling if not properly mitigated.

The median filter is a robust, non-parametric technique widely used for outlier detection due to its insensitivity to extreme values [70]. Given a discrete RSSI time series $\{y_i\}_{i=1}^{m}$, a sliding window of odd length $2k+1$ is centered at each observation. The local median is computed as

$$\lambda_i = \text{median}\left(y_{i-k}, \dots, y_i, \dots, y_{i+k}\right). \tag{1}$$

An observation is classified as an outlier if its deviation from the local median exceeds a predefined threshold:

$$|y_i - \lambda_i| > T, \tag{2}$$

where T can be selected empirically or defined in a robust statistical sense. Detected outliers are mitigated by replacing them with the local median λ_i, thereby preserving the underlying signal structure while suppressing impulsive noise. In contrast, the mean filter, defined as

$$\mu_i = \frac{1}{2k+1}\sum_{j=i-k}^{i+k} y_j, \tag{3}$$

is highly sensitive to extreme values. A single outlier within the window can significantly bias the mean, reducing its effectiveness for outlier detection and potentially propagating errors into subsequent processing stages. Mean filtering is therefore more suitable for smoothing Gaussian-distributed noise after outliers have already been removed, rather than for outlier identification itself.

For RSSI measurements, which typically exhibit non-Gaussian behavior with sporadic spikes, the median filter is prioritized over the mean filter due to its robustness and edge-preserving characteristics. This property is particularly important for BLE signals, where abrupt RSSI fluctuations may arise from transient environmental effects rather than gradual noise processes. Consequently, median-based outlier detection provides a reliable foundation for subsequent stochastic modeling, including autocorrelation analysis and variance component estimation.

2.2. Stochastic modeling for RSSI measurements

2.2.1. Cofactor matrix determination using ACF and PACF evaluation

The initial step involves identifying the noise model of the RSSI measurements, which is essential for accurately estimating the distance between BLE beacons and the receiver. To this end, the ACF and PACF are employed. Let us assume a stationary time series $\mathbf{y} = [y_1, y_2, \dots, y_m]^{\mathsf{T}}$ with mean $\mu_y = \mathbb{E}[y_t]$ and variance $\sigma_y^2 = \text{var}(y_t)$. The theoretical autocovariance function is defined as [71]:

$$C_y(\tau) = \text{cov}(y_t, y_{t-\tau}) = \mathbb{E}\left[(y_t - \mu_y)(y_{t-\tau} - \mu_y)\right], \tag{4}$$

where τ denotes the time lag. The autocorrelation function is defined as

$$R_y(\tau) = \text{corr}(y_t, y_{t-\tau}) = \frac{\mathbb{E}[(y_t - \mu_y)(y_{t-\tau} - \mu_y)]}{\sigma_y^2}. \tag{5}$$

For a zero-mean process ($\mu_y = 0$) with unit variance ($\sigma_y^2 = 1$), it follows that

$$C_y(\tau) = R_y(\tau). \tag{6}$$

The least squares method or maximum likelihood method can be used to estimate the auto covariance and auto-correlation function of time series. The sample autocovariance function can be estimated as

$$\hat{C}_y(\tau) = \frac{1}{m-\tau}\sum_{i=1}^{m-\tau}(y_i - \mu_y)(y_{i+\tau} - \mu_y), \qquad \tau = 0, 1, \dots, m-1. \tag{7}$$

The empirical autocorrelation function (sample ACF) is then given by

$$\hat{R}_y(\tau) = \frac{\sum_{i=1}^{m-\tau}(y_i - \mu_y)(y_{i+\tau} - \mu_y)}{\sum_{i=1}^{m}(y_i - \mu_y)^2}, \qquad \tau = 0, 1, \dots, m-1. \tag{8}$$

The PACF measures the direct relationship between a time series observation and a previous observation after removing the linear influence of intervening observations [72,73]. It is particularly useful for identifying the order of an autoregressive (AR) process [74]. Accordingly, the RSSI noise is modeled as a stationary AR(2) process as follows:

$$y_t = \beta_1 y_{t-1} + \beta_2 y_{t-2} + e_t, \qquad t = 3, \dots, m, \tag{9}$$

where $e_t \sim \mathcal{N}(0, \sigma_e^2)$ denotes white Gaussian noise, and β_1 and β_2 are the autoregressive coefficients. The stationarity condition requires that the roots of

$$1 - \beta_1 z - \beta_2 z^2 = 0 \tag{10}$$

lie outside the unit circle, where z denotes a complex number. For a stationary AR(2) process, the autocovariances satisfy the Yule–Walker equations. Once the autoregressive order $p = 2$ has been identified from the cutoff behavior of the PACF, the AR(2) coefficients can be estimated directly from the sample ACF using the Yule–Walker relations. The theoretical autocorrelations $\rho_k = R_y(k)$ satisfy

$$\rho_1 = \beta_1 + \beta_2 \rho_1, \tag{11}$$

$$\rho_2 = \beta_1 \rho_1 + \beta_2. \tag{12}$$

Replacing the theoretical autocorrelations with their sample estimates, $\hat{\rho}_1 = \hat{R}_y(1)$ (ACF at lag 1) and $\hat{\rho}_2 = \hat{R}_y(2)$ (ACF at lag 2), yields closed-form expressions for the AR(2) coefficients:

$$\beta_2 = \frac{\hat{\rho}_2 - \hat{\rho}_1^2}{1 - \hat{\rho}_1^2}, \tag{13}$$

$$\beta_1 = \hat{\rho}_1 \left(1 - \beta_2\right). \tag{14}$$

These estimates provide a computationally efficient and statistically consistent initialization of the AR(2) noise model. The resulting coefficients are subsequently used to derive the autocovariance sequence and to construct the Toeplitz cofactor matrix of the RSSI observations for stochastic modeling and LS-VCE analysis. The corresponding Yule–Walker equations for the autocovariances are given by

$$\gamma_1 = \beta_1 \gamma_0 + \beta_2 \gamma_1, \tag{15}$$

$$\gamma_2 = \beta_1 \gamma_1 + \beta_2 \gamma_0, \tag{16}$$

$$\gamma_0 = \beta_1 \gamma_1 + \beta_2 \gamma_2 + \sigma_e^2, \tag{17}$$

where $\gamma_k = \mathrm{cov}(y_t, y_{t-k})$. Solving these equations yields explicit expressions for the first three autocovariances:

$$\gamma_0 = \frac{\sigma_e^2 (1 - \beta_2)}{(1 + \beta_2)\left[(1 - \beta_2)^2 - \beta_1^2\right]}, \tag{18}$$

$$\gamma_1 = \frac{\beta_1}{1 - \beta_2} \gamma_0, \tag{19}$$

$$\gamma_2 = \left(\frac{\beta_1^2}{1 - \beta_2} + \beta_2 \right) \gamma_0. \tag{20}$$

For lags $k \geq 3$, the autocovariance function follows the recursive relation

$$\gamma_k = \beta_1 \gamma_{k-1} + \beta_2 \gamma_{k-2}. \tag{21}$$

Based on this autocovariance structure, the cofactor matrix of the RSSI observations is constructed as a symmetric Toeplitz matrix:

$$\mathbf{Q}_y = \begin{pmatrix} \gamma_0 & \gamma_1 & \gamma_2 & \cdots & \gamma_{m-1} \\ \gamma_1 & \gamma_0 & \gamma_1 & \cdots & \gamma_{m-2} \\ \gamma_2 & \gamma_1 & \gamma_0 & \cdots & \gamma_{m-3} \\ \vdots & \vdots & \vdots & \ddots & \vdots \\ \gamma_{m-1} & \gamma_{m-2} & \gamma_{m-3} & \cdots & \gamma_0 \end{pmatrix}. \tag{22}$$

This AR(2)-based cofactor matrix explicitly accounts for second-order temporal correlations in the RSSI measurements, enabling a more realistic stochastic representation of colored noise. Compared with the AR(1) model, the AR(2) formulation is capable of capturing more complex correlation patterns, including oscillatory behavior induced by multipath propagation and environmental persistence. Consequently, its integration within the LS-VCE framework yields a higher log-likelihood and improved parameter uncertainty assessment. Also, the behaviors of the ACF and PACF can provide a comprehensive view of the noise model underlying the time series of measurement [75]. If the ACF plot exhibits a gradual decay, while the PACF cuts off after p lags, the noise model is identified as an autoregressive (AR) model of order p. Conversely, if the ACF plot cuts off after q lags and the PACF shows a gradual decay, the noise model corresponds to a moving average (MA) model of order q. Furthermore, if both the ACF and PACF plots display a gradual decay, the noise model is characterized as an autoregressive moving average (ARMA) model, with orders p and q respectively. Moreover, understanding the ACF in the time domain is mathematically equivalent to understanding the power spectral density (PSD) in the frequency domain, and the two are inherently related. The PSD of a discrete-time random process can be obtained from the Fourier transform of its autocorrelation function, according to the Wiener–Khinchin theorem. For a finite RSSI time series $\{y_i\}_{i=1}^m$, the sample autocorrelation function is estimated as

$$\hat{R}_y(\tau) = \frac{1}{m} \sum_{i=1}^{m-\tau} y_i \, y_{i+\tau}, \qquad \tau = 0, 1, \ldots, m-1. \tag{23}$$

The PSD estimate is then obtained by applying the discrete Fourier transform (DFT) to the autocorrelation sequence:

$$S_y(k) = \sum_{\tau=-(m-1)}^{m-1} \hat{R}_y(\tau) \exp\left(-j \frac{2\pi}{m} k\tau\right), \qquad k = 0, 1, \ldots, m-1. \tag{24}$$

Equivalently, the PSD can be expressed in periodogram form as

$$S_y(k) = \frac{1}{m \, \Delta t} \left| Y(k) \right|^2, \tag{25}$$

where $Y(k)$ denotes the discrete Fourier transform of the RSSI measurements, defined by

$$Y(k) = \Delta t \sum_{i=1}^{m} y_i \exp\left(-j \frac{2\pi}{m} k(i-1)\right), \qquad k = 0, 1, \ldots, m-1. \tag{26}$$

The equivalence between the PSD obtained from the Fourier transform of the autocorrelation function and the squared magnitude of the signal DFT follows directly from the Wiener–Khinchin theorem.

The ACF provides a measure of how a signal correlates with a delayed version of itself over time, offering insight into the temporal structure and properties of the signal. On the other hand, the PSD describes how the power of a signal is distributed across different frequencies, providing information about its frequency characteristics. These two representations are connected through the Wiener–Khinchin theorem, which states that the Fourier transform of the ACF yields the PSD, and vice versa. Therefore, knowledge of one domain (time or frequency) allows for a complete understanding of the other, as both domains offer complementary perspectives of the signal's behavior [76]. The PSD of signals provides a representation of the stochastic behavior of BLE measurement within the frequency domain. When a line is fitted to the PSD plot, the slope of this line (slope index) offers insight into the underlying noise characteristics of the measurement process. Specifically, if the slope of the line is zero, it indicates that all frequencies contribute equally to the variance of the signal, suggesting that the noise is purely random and can be classified as white-noise. Conversely, a non-zero slope signifies that the noise exhibits frequency-dependent behavior, with certain frequencies contributing more significantly to the signal's variance. This type of noise is known as colored-noise, where the noise characteristics are more structured and less random than white-noise. The greater the slope deviates from zero, the more the noise depends on frequency.

2.2.2. Covariance matrix determination for all measurements

It encompasses both functional and stochastic parts, which are essential for the optimal estimation of parameters. Subsequently, the first and second terms are referred to as the functional model and the stochastic model, respectively.

$$\mathbf{y} = \mathbf{A}\mathbf{x} + \mathbf{e}, \qquad \mathbb{D}[\mathbf{y}] = \mathbf{Q}_y \tag{27}$$

where $\mathbf{y} \in \mathbb{R}^m$ is a vector of m measurement, $\mathbf{x} \in \mathbb{R}^n$ is a vector of n unknown parameters, $\mathbf{A} \in \mathbb{R}^{(m \times n)}$ is a given design matrix,

$\mathbf{e} \in \mathbb{R}^m$ is a vector of m residuals (errors) and $\mathbf{Q}_y \in \mathbb{R}^{m\times m}$ is the positive semi-definite covariance matrix of observable y. Also, $\mathbb{D}$ is the dispersion operator. In our problem, the functional model linking RSSI and distances is as follows [21]:

$$\mathrm{RSSI}_{k,i} = -10\ \nu \log_{10} d_k - \varepsilon \tag{28}$$

where i denotes the ith observation of the RSSI, and d_k is the kth distance corresponding to the RSSI measurement. The variable ν refers to the environmental factor, a constant that accounts for the specific environmental conditions affecting signal propagation. Additionally, ε represents the maximum power coefficient, which characterizes the strength of the signal at a reference distance, typically under ideal conditions. These parameters are essential for accurate indoor positioning and distance estimation in BLE-based wireless systems. In other words, we have

$$\mathrm{RSSI}_{k,i} = -10\ \nu \log_{10} \sqrt{\left(x_{s_k} - x_r\right)^2 + \left(y_{s_k} - y_r\right)^2 + \left(z_{s_k} - z_r\right)^2} - \varepsilon + e \tag{29}$$

where $\left[x_{s_k}\, y_{s_k}\, z_{s_k}\right]^T$ is the position of kth BLE beacons, and $\left[x_r\ y_r\ z_r\right]^T$ is the receiver position. For estimating the mentioned parameters, the given design matrix and the vector of two unknown parameters is

$$\mathbf{A} = \begin{pmatrix} -10\log d_1 & -1 \\ -10\log d_2 & -1 \\ \vdots & \vdots \\ -10\log d_m & -1 \end{pmatrix}, \mathbf{x} = \begin{pmatrix} \nu \\ \varepsilon \end{pmatrix}. \tag{30}$$

Given that shorter distances, characterized by stronger signal strength, typically exhibit higher measurement accuracy compared to longer distances, where signals are weaker and subject to greater variability, the LS-VCE technique was employed [66,67]. This method can be used to assign appropriate weights to each distance measurement, thereby ensuring that the more accurate, shorter-distance measurement had a greater influence on the calibration process. We assume the measured distance covariance matrix is as follows:

$$\mathbb{D}[\mathbf{y}] = \mathbf{Q}_y = \sum_{i=1}^{p} \sigma_i^2 \mathbf{Q}_i \tag{31}$$

where i denotes the type of measurements, σ_i^2 is the variance factor of each type of measurement, and $\mathbf{Q}_i$ is the co-factor matrices which are obtained from the previous section, and p is the number of different measurement types, each having a different variance. LS-VCE was developed by Teunissen and Amiri-Simkooei [66], and applied to assess the noise of GPS position time series [69,77,78]. The LS-VCE pseudo-code is presented in Algorithm 1.

2.3. Functional modeling for RSSI measurements

After the computation of the design matrix and covariance matrix of all measurement, the BLUE of the unknown parameters is as follows [79]:

$$\hat{\mathbf{x}} = \left(\mathbf{A}^T \mathbf{Q}_y^{-1} \mathbf{A}\right)^{-1} \mathbf{A}^T \mathbf{Q}_y^{-1} \mathbf{y}. \tag{32}$$

Finally, the estimated measurement and residuals are

$$\hat{\mathbf{y}} = \mathbf{P}_A \mathbf{y},\ \hat{\mathbf{e}} = \mathbf{P}_A^{\perp} \mathbf{y} \tag{33}$$

where $\mathbf{P}_A = \mathbf{A}\left(\mathbf{A}^T \mathbf{Q}_y^{-1} \mathbf{A}\right)^{-1} \mathbf{A}^T \mathbf{Q}_y^{-1}$ and $\mathbf{P}_A^{\perp} = \mathbf{I} - \mathbf{P}_A$ are two orthogonal projectors. The covariance matrices of estimated parameters are as follows:

$$\mathbf{Q}_{\hat{x}} = \left(\mathbf{A}^T \mathbf{Q}_y^{-1} \mathbf{A}\right)^{-1}. \tag{34}$$

Algorithm 1: Pseudo-code for LS-VCE

Input: Design matrix $\mathbf{A}$; measurement vector $\mathbf{y}$; cofactor matrices $\mathbf{Q}_k$, $k = 1, \ldots, p$; initial variance components $\boldsymbol{\sigma}^0$; tolerance ϵ.
Output: Estimated variance components $\hat{\boldsymbol{\sigma}}$ and covariance matrix $\mathbf{Q}_{\hat{\sigma}}$.

$i \leftarrow 0$;
Compute $\mathbf{Q}_y = \sum_{k=1}^{p} \sigma_k^2 \mathbf{Q}_k$;
Invert $\mathbf{Q}_y$;
Compute $\mathbf{P}_A^{\perp} = \mathbf{I} - \mathbf{A}(\mathbf{A}^T \mathbf{Q}_y^{-1} \mathbf{A})^{-1} \mathbf{A}^T \mathbf{Q}_y^{-1}$;
Compute residuals $\hat{\mathbf{e}} = \mathbf{P}_A^{\perp} \mathbf{y}$;
Compute $\mathbf{N}_{ij} = \frac{1}{2} \mathrm{tr}(\mathbf{Q}_y^{-1} \mathbf{P}_A^{\perp} \mathbf{Q}_i \mathbf{Q}_y^{-1} \mathbf{P}_A^{\perp} \mathbf{Q}_j)$;
Compute $\mathbf{l}_i = \frac{1}{2} \hat{\mathbf{e}}^T \mathbf{Q}_y^{-1} \mathbf{Q}_i \mathbf{Q}_y^{-1} \hat{\mathbf{e}}$;
Solve $\mathbf{N}\hat{\boldsymbol{\sigma}} = \mathbf{l}$;
while $\|\boldsymbol{\sigma}^i - \hat{\boldsymbol{\sigma}}\|_{\mathbf{Q}_{\hat{\sigma}}^{-1}} > \epsilon$ **do**
  $i \leftarrow i + 1$;
  $\boldsymbol{\sigma}^i \leftarrow \hat{\boldsymbol{\sigma}}$;
$\mathbf{Q}_{\hat{\sigma}} = \mathbf{N}^{-1}$;

In this problem, the covariance matrix of estimated parameters is as follows:

$$\mathbf{Q}_{\hat{x}} = \begin{pmatrix} \sigma_\nu^2 & \sigma_{\nu\varepsilon} \\ \sigma_{\varepsilon\nu} & \sigma_\varepsilon^2 \end{pmatrix} \tag{35}$$

where $\pm\sigma_\nu$ and $\pm\sigma_\varepsilon$ denote the precision of the functional model parameters, and $\sigma_{\nu\varepsilon}$ denotes the estimated covariance. This estimated precision can be propagated to the receiver's position components, which represent the precision of the indoor positioning solution, by applying the law of error propagation, as comprehensively presented in [18]. The joint stochastic and functional modeling framework is illustrated in Fig. 1.

2.4. Uncertainty analysis and maximum log-likelihood estimation

Uncertainty analysis is an essential component of RSSI-based modeling, as it provides a quantitative assessment of the reliability of the estimated model parameters and the resulting distance estimates. In the proposed framework, uncertainty analysis is performed following the stochastic and functional modeling stages to evaluate how measurement noise, including time-correlated dependencies induced by multipath propagation, propagates into the estimated RSSI–distance model parameters. To provide a practical interpretation of the RSSI reconstruction accuracy, the corresponding distance uncertainty is estimated using the logarithmic RSSI–distance model. Solving Eq. (28) for distance yields

$$d = 10^{\frac{\varepsilon + \mathrm{RSSI}}{-10\nu}}. \tag{36}$$

The effect of RSSI reconstruction errors on distance estimation can be quantified through first-order error propagation. Taking the natural logarithm of Eq. (36) and differentiating with respect to RSSI gives

$$\frac{\partial \ln d}{\partial \mathrm{RSSI}} = -\frac{\ln(10)}{10\nu}. \tag{37}$$

Consequently, the relative distance uncertainty can be approximated as

$$\frac{\sigma_d}{d} \approx \frac{\ln(10)}{10\nu} \sigma_{\mathrm{RSSI}}, \tag{38}$$

where σ_{RSSI} represents the RSSI reconstruction error, expressed here by the corresponding RMSE value, and σ_d denotes the induced distance uncertainty. Eq. (38) demonstrates that the distance error grows linearly with the RSSI error and inversely with the path-loss exponent. For typical BLE propagation environments, where ν generally ranges from 2 to 4, the obtained RSSI reconstruction accuracies correspond to relative

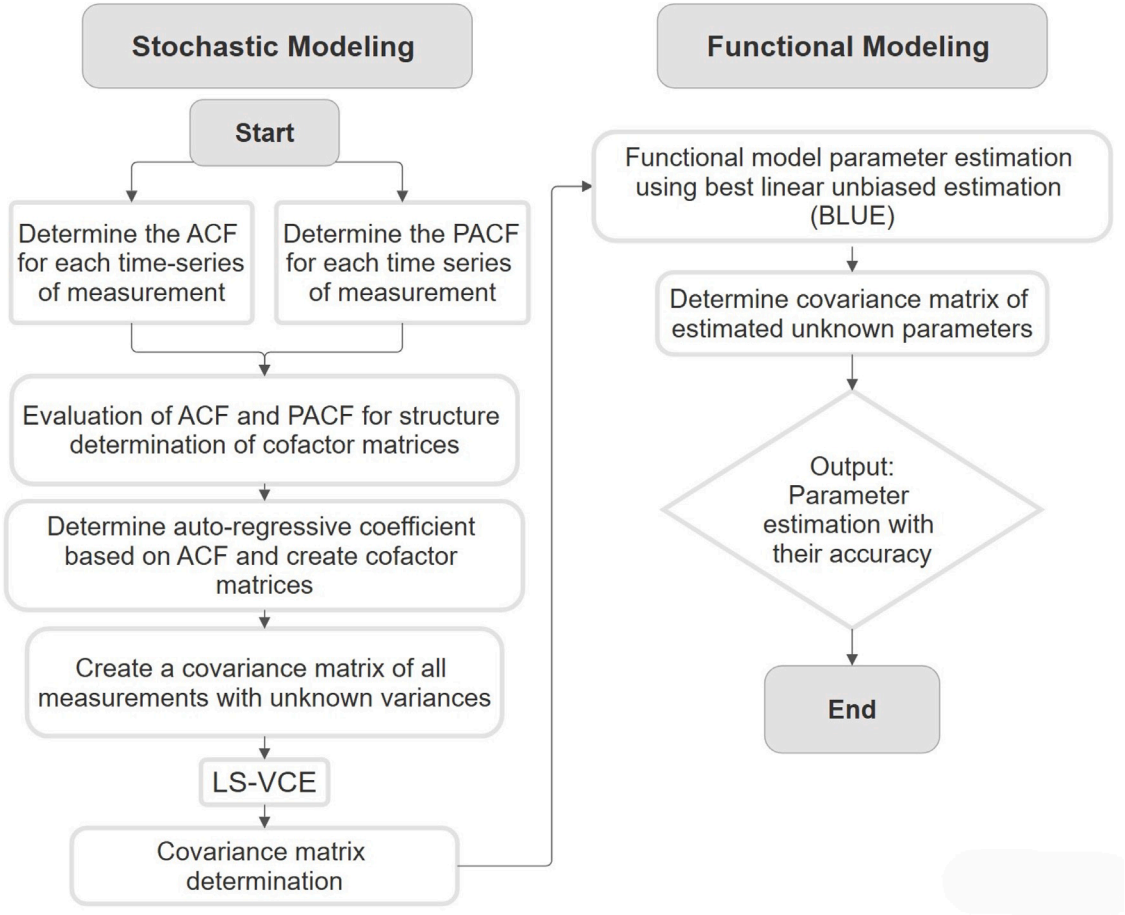


Fig. 1. Stochastic and functional modeling algorithm flowchart diagram.

distance uncertainties of approximately 6–13% for RMSE values near 1 dBm and 15–25% for RMSE values around 2–2.5 dBm. These values provide an intuitive interpretation of the practical ranging performance associated with the reconstructed RSSI measurements.

A statistically rigorous selection of the most appropriate stochastic model can be achieved via the maximum log-likelihood criterion. Let $\mathbf{y} \in \mathbb{R}^m$ denote the observation vector and $\boldsymbol{\theta}$ the parameter vector of a candidate stochastic model $\mathcal{M}_i$, characterized by covariance matrix $\mathbf{Q}_y$. Assuming Gaussianity, the log-likelihood function is given by

$$\ell_i(\boldsymbol{\theta}) = -\frac{1}{2}\left[m\ln(2\pi) + \ln\left|\mathbf{Q}_y\right| + \mathbf{y}^\top \mathbf{Q}_y^{-1}\mathbf{y}\right]. \tag{39}$$

The MLE of $\hat{\boldsymbol{\theta}}_i$ is obtained as

$$\hat{\boldsymbol{\theta}}_i = \arg\max_{\boldsymbol{\theta}} \ \ell_i(\boldsymbol{\theta}). \tag{40}$$

Substituting $\hat{\boldsymbol{\theta}}_i$ into the log-likelihood yields the maximized value

$$\ell_i^{\max} = \ell_i(\hat{\boldsymbol{\theta}}_i). \tag{41}$$

For a set of competing models $\{\mathcal{M}_1, \ldots, \mathcal{M}_K\}$, the optimal stochastic model is selected according to

$$\mathcal{M}^\star = \arg\max_{\mathcal{M}_i} \ \ell_i^{\max}. \tag{42}$$

Accordingly, the model that attains the highest log-likelihood value provides the best statistical representation of the underlying stochastic process, assuming comparable model complexity.

Together, uncertainty analysis and the MLE provide a comprehensive statistical validation of the proposed modeling framework, ensuring that both the estimated parameters and their associated uncertainties are reliable and physically meaningful.

3. Case study

A case study was conducted using two selected types of BLE beacons to perform stochastic and functional modeling of RSSI measurements, with the objective of accurately estimating the parameters of the RSSI–distance model. Four precise fixed distances between BLE beacons (as transmitters) and a Samsung Galaxy S22+ (as a receiver) are measured. These fixed distances are initially realized using advanced surveying equipment. These measurement were collected over a series of 20-minute intervals at a sampling rate of 0.5 Hz, conducted in a controlled outdoor environment at the Université Laval campus in Quebec City, Quebec, Canada. This environment was specifically chosen for its minimal signal interference, particularly the absence of multipath effects, which is crucial for ensuring the accuracy and reliability of the noise-assessing process. For the experiment, four arbitrary distances have been adopted based on the nominal coverage of the BLEs. The measurement were taken at fixed distances of 1, 3, 5, and 10 m, thereby encompassing a range of near-field to far-field scenarios. The mentioned methodology was carried out for two distinct types of BLE beacons, each exhibiting unique characteristics and signal behavior. The resulting data were used to perform a comprehensive mathematical framework that accounts for the performance of both beacon types, as depicted in Figs. 2, and 3, respectively.

3.1. Case study 1

The first beacon, whose measurement were taken to identify the model, is introduced here. The Screw-ON Bluetooth® IT002 beacon represents the most advanced generation of Bluetooth beacons developed by Tatwah company. It is fully compatible with the Bluetooth®



Fig. 2. Tatwah's IT002 Bluetooth Low Energy beacon.

5.0 standard and is meticulously designed to meet the diverse requirements of various applications, including asset tracking, logistics, inventory management, and predictive maintenance. Thanks to its highly optimized and ultra-low power consumption, this beacon ensures exceptional battery longevity. Additionally, it features the ability to replace its CR2032 battery, further enhancing its practicality and cost-effectiveness. Equipped with a high-precision accelerometers sensor, the beacon is capable of detecting a wide range of movements, including vibrations, shocks, and specific impacts such as falls. The parameters of the accelerometers can be easily configured to suit the specific needs of the application, offering flexibility for a variety of use cases. All configuration settings for the beacon can be conveniently updated over the air through a dedicated profile service, ensuring ease of management and customization. Furthermore, a secure operational mode is available, utilizing an AES-128 encryption algorithm to guarantee data protection. For added functionality, an optional NFC (Near Field Communication) feature can be integrated, providing the ability to deliver additional information about the asset, such as its manual, last maintenance date, or location. This NFC functionality also enables a simplified pairing process for enhanced user experience.

The experiment was conducted using four fixed distances between the beacon, acting as the signal transmitter, and a Samsung Galaxy S22+ smartphone, serving as the receiver. Following data collection at each distance, the RSSI observations were processed using a median filter, whereby samples identified as outliers were replaced by the median value within a predefined local window. Subsequently, the ACF and PACF were computed for each RSSI time series. Based on these analyses, the corresponding β_1 and β_2 parameters were estimated, followed by the estimation of γ_0, γ_1, and γ_2 from the ACF. These parameters were then used to construct the cofactor matrices required for stochastic modeling.

3.2. Case study 2

The second beacon, which is used, is introduced here. The Industrial Screwable Bluetooth® IT008 beacon represents the latest generation of Bluetooth® beacons engineered by Tatwah company. This cutting-edge device is also fully compatible with the Bluetooth® 5.0 standard and has been meticulously designed to meet the diverse and evolving requirements of a wide range of applications, including asset tracking, logistics, inventory management, and predictive maintenance. With



Fig. 3. Tatwah's IT008 Bluetooth Low Energy beacon.

its highly optimized and ultra-low power consumption, the IT008 tag ensures exceptional, industry-leading battery life. Moreover, it offers the practical advantage of being powered by replaceable AA batteries, enabling ease of maintenance and prolonged usage in demanding environments. Equipped with a high-precision accelerometers sensor, the beacon is capable of detecting a wide array of movements, including vibrations, shocks, and specific events such as falls. The parameters of the accelerometers are fully configurable, allowing them to be fine-tuned to meet the precise needs of the particular application, ensuring maximum accuracy and reliability. All configuration settings for the beacon can be updated remotely, over the air, through a dedicated profile service, providing seamless management and flexibility. Additionally, a secure operational mode is available, employing an AES-128 cryptographic algorithm to ensure the highest standards of data security and protection. For enhanced functionality, the beacon can be optionally equipped with an NFC feature. This feature enables the transmission of additional information regarding the asset, such as its manual, the last maintenance date, or its precise location. The NFC functionality also facilitates a simplified pairing process, further streamlining the user experience and improving operational efficiency.

In Case Study II, the same experimental procedure as in Case Study I was adopted, using four predefined distances between the BLE beacon (transmitter) and a Samsung Galaxy S22+ smartphone (receiver). After RSSI data acquisition, the measurements were processed using a median filter to mitigate outliers by replacing anomalous values with the median of their local neighborhood. The filtered time-series were then analyzed using the ACF and PACF to characterize their temporal dependence structure. Based on these analyses, the parameters β_1 and β_2 were estimated. Subsequently, the covariance-related parameters γ_0, γ_1, and γ_2 were derived from the ACF and used to construct the stochastic cofactor matrices required for subsequent modeling.

After creation of cofactor matrices for all types of measurements, for both beacons, we have a same covariance matrix structure as follows:

$$\mathbf{Q}_y = \sigma_1^2\mathbf{Q}_1 + \sigma_3^2\mathbf{Q}_3 + \sigma_5^2\mathbf{Q}_5 + \sigma_{10}^2\mathbf{Q}_{10} \tag{43}$$

where four fixed distances are measured between the mentioned beacons and a smartphone as a receiver. Also, the cofactor matrices and their associated variance components are estimated according to the methodology introduced in this study.

4. Results and discussion

This section presents the results of the stochastic and functional modeling for the two case studies, together with the MLE results obtained for four candidate noise models. The RSSI measurement at distances of 1, 3, 5, and 10 m are presented for both beacons in Figs. 4 and 5, respectively. In these figures, outliers in each time series were identified and replaced using a median filter, whereby each outlier was

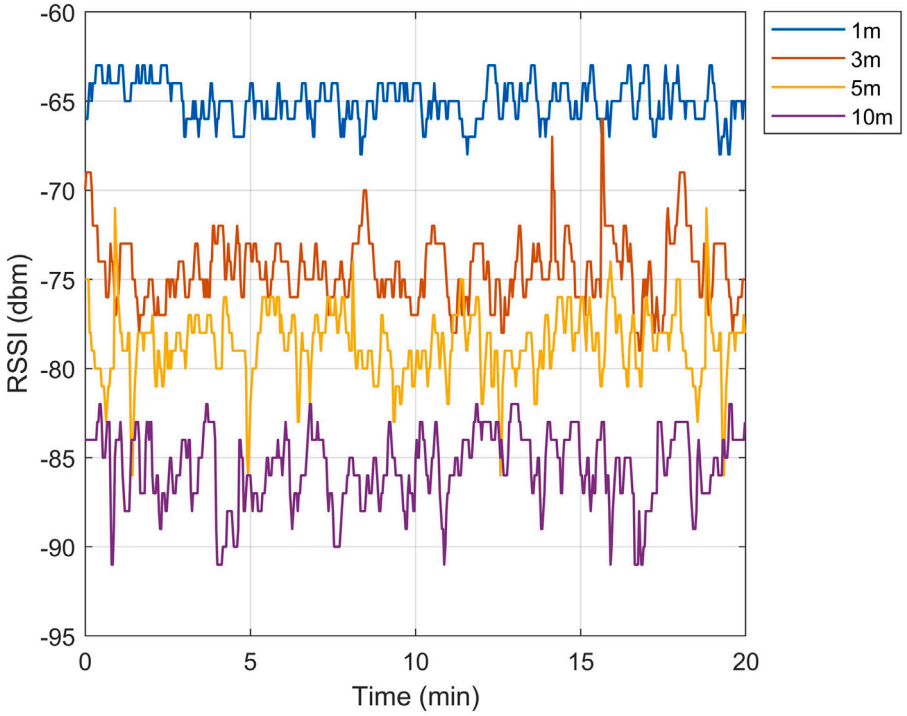


Fig. 4. All RSSI measurement of the IT002 beacon over a 20-minute duration at fixed distances.

Table 2
Estimated AR(2) coefficients obtained from RSSI measurements at different distances.

Distance (m)	IT002 beacon		IT008 beacon	
	β_1	β_2	β_1	β_2
1	0.9707	−0.1375	0.7426	−0.0193
3	1.0067	−0.1565	1.1998	−0.3757
5	1.0645	−0.2821	1.1668	−0.3241
10	1.1992	−0.3455	1.0110	−0.1347

Table 3
Estimated autocovariance coefficients obtained from the ACF analysis of RSSI measurements for the IT002 and IT008 beacons at different distances.

Distance (m)	IT002 beacon			IT008 beacon		
	γ_0	γ_1	γ_2	γ_0	γ_1	γ_2
1	1.2615	1.0765	0.8716	0.2578	0.1878	0.1345
3	3.6630	3.1885	2.6366	3.9939	3.4833	2.6789
5	3.8418	3.1896	2.3114	3.2312	2.8475	2.2755
10	4.4736	3.9871	3.2355	4.7222	4.2073	3.6173

substituted with the median of its neighboring observations. Also, the PSD estimate derived from the RSSI measurement has been computed for all measurement, demonstrating that the slope of the fitted line is non-zero. The PSD estimate reveals that the correlation between the noise is not entirely random, as would be characteristic of white-noise. Instead, it suggests the presence of a random process that governs the observed dependency, indicative of colored-noise. This type of noise exhibits a structured correlation over time, distinguishing it from the unpredictability of white-noise and highlighting its inherent patterns. The PSD of RSSI measurements for both the IT002 and IT008 BLE beacons at distances of 1, 3, 5, and 10 m is depicted in Fig. 6.

The estimated ACF and PACF of the RSSI measurements, obtained at fixed distances of 1, 3, 5, and 10 m, are illustrated in Fig. 7 for the IT002 beacon and in Fig. 8 for the IT008 beacon.

As described in Section 2, noise characterization, which is required for the construction of the measurement cofactor matrix, constitutes a fundamental component of the stochastic modeling framework. To this end, the ACF and partial ACF were first applied to all RSSI measurements. Based on these analyses, the corresponding β_1 and β_2 parameters associated with each cofactor matrix were estimated and are summarized in Table 2. Subsequently, the covariance function parameters γ_0, γ_1, and γ_2 were derived for each cofactor matrix, with the results presented in Table 3.

Following the stochastic characterization, variance components for all measurements in both case studies were estimated using the LS-VCE method, with the results reported in Table 4. The parameters of the

Table 4
Estimated variance components obtained using the LS-VCE method for the IT002 and IT008 beacons.

Variance component	IT002 beacon	IT008 beacon
$\hat{\sigma}_1$ (dBm)	1.2609	0.2583
$\hat{\sigma}_3$ (dBm)	3.5510	3.8125
$\hat{\sigma}_5$ (dBm)	3.8188	3.1757
$\hat{\sigma}_{10}$ (dBm)	4.4190	4.7573
Number of iterations	3	3

RSSI–distance functional model and their associated precision measures were subsequently estimated using the BLUE method and are presented in Table 5. The performance of the proposed framework was evaluated by computing the root mean square error (RMSE) between the reconstructed RSSI signals and the corresponding raw measurements. The resulting RMSE values are summarized in Table 6.

Also, the estimated log-likelihood values for four candidate stochastic models indicate that the adopted AR(2) model achieves the maximum value, thereby confirming its statistical consistency and suitability as the preferred representation. Table 7 summarizes the log-likelihood results for the white-noise, AR(1), AR(2), and AR(3) models.

Finally, the RSSI signals reconstructed using the proposed model are illustrated in Figs. 9 and 10 for the first and second case studies, respectively.

Our experimental results indicate that different BLE beacons exhibit distinct characteristics. For example, the IT002 beacon shows lower

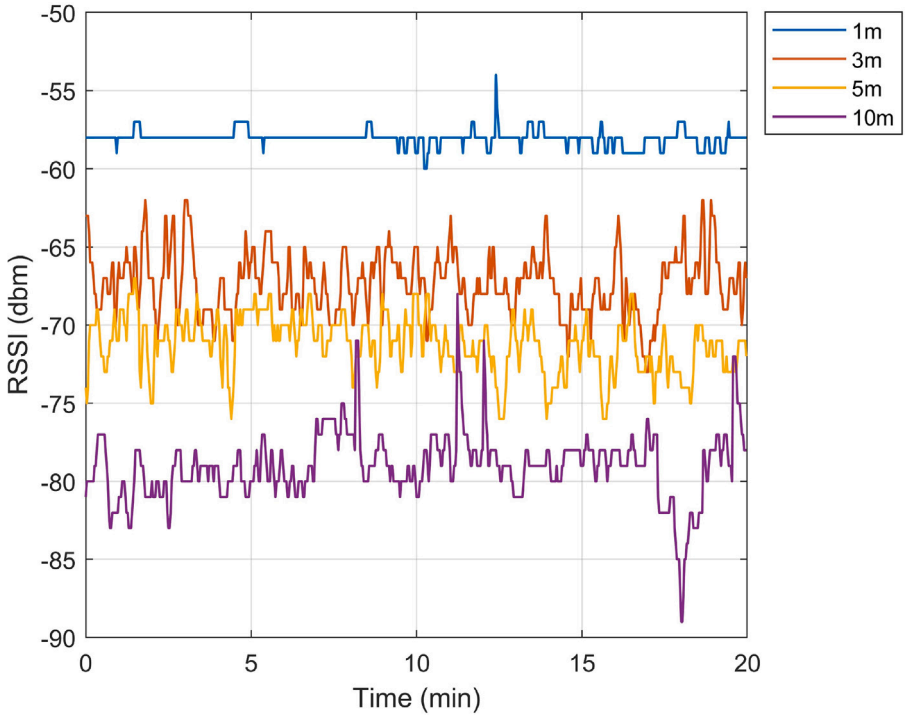


Fig. 5. All RSSI measurement of the IT008 beacon over a 20-minute duration at fixed distances.

Table 5
Estimated RSSI–distance model parameters and their associated precision measures for the IT002 and IT008 beacons.

Parameter	IT002 beacon	IT008 beacon
ν	2.0044	1.9964
ε (dBm)	64.9632	58.0342
σ_ν	0.0315	0.0260
σ_ε (dBm)	0.1563	0.0519
$\sigma_{\nu\varepsilon}$	−0.0033	−0.0003

Table 6
RMSE of the reconstructed RSSI signals.

Distance (m)	IT002 RMSE (dBm)	IT008 RMSE (dBm)
1	1.1242	0.5079
3	1.9144	2.0140
5	1.9890	1.9575
10	2.1912	2.4071

Table 7
Log-likelihood values for four stochastic models used in RSSI noise characterization.

Stochastic model	IT002 beacon	IT008 beacon
White noise	-5.774×10^3	-5.447×10^3
AR(1)	-3.066×10^3	-2.649×10^3
AR(2)	-3.065×10^3	-2.648×10^3
AR(3)	-3.099×10^3	-2.698×10^3

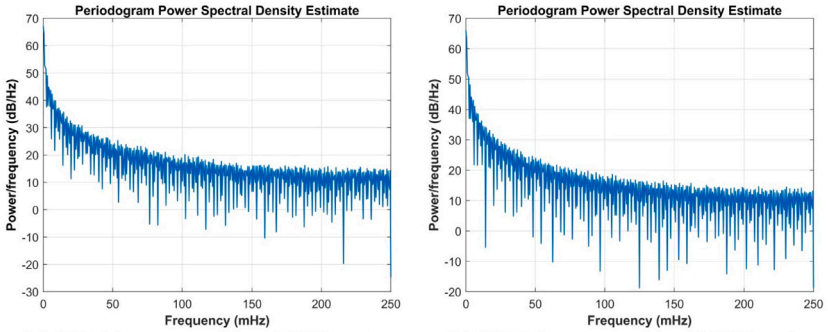
maximum transmission power compared to the IT008, reflecting its design as a standard device versus the industrial-grade IT008. This nominal difference aligns with our observations, whereas the environmental factor remains approximately the same across both beacons, consistent with the uniform experimental environment. The proposed modeling process can be applied to any BLE beacon to reveal device-specific characteristics and guide parameter estimation for accurate distance estimation.

We also observe that increasing the separation between beacon and receiver leads to higher measurement fluctuations, elevated variance, and stronger temporal correlation among RSSI measurements, as quantified by the β_1 and β_2 parameter. Multi-path effects are amplified in indoor environments, particularly in spaces with dense and complex structural layouts, further increasing measurement correlation and influencing positioning accuracy. These results highlight the critical role of environment and structural configuration in system performance.

The AR(2)-based stochastic model adequately captures the temporal correlation structure of RSSI noise, as verified through residual whiteness tests and MLE. Incorporating the resulting covariance model into the weighted least squares estimation process produces statistically efficient parameter estimates and realistic uncertainty quantification. The reconstructed RSSI signals achieved RMSE values of 1.12 dBm and 0.50 dBm for the IT002 and IT008 beacons, respectively, at a distance of 1 m, increasing to 2.19 dBm and 2.40 dBm at 10 m. These values correspond to relative distance uncertainties of approximately 6–13% at 1 m and 15–25% at 10 m, confirming the capability of the proposed stochastic–functional framework to accurately characterize BLE RSSI measurements and support reliable distance estimation.

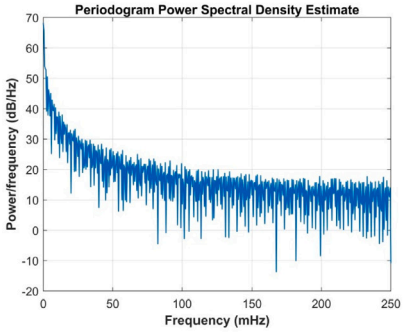
The comprehensive stochastic–functional modeling framework developed in this study is broadly applicable to a wide range of operational scenarios. It can be readily extended to dynamic environments, different types of BLE beacons and receivers, varying receiver–beacon geometries, diverse indoor layouts, and different coverage distances. By explicitly accounting for both the functional relationship and the stochastic characteristics of RSSI measurements, the proposed framework facilitates a systematic and rigorous characterization of RSSI behavior. Consequently, it provides a robust basis for reliable indoor positioning performance under heterogeneous and realistic operating conditions.

Finally, the findings of this study provide actionable guidance for the optimal deployment of BLE beacons. By first estimating the effective coverage based on the maximum transmission power and subsequently evaluating distance estimation precision, system designers can strategically determine beacon placement to maximize positioning accuracy and reliability. These insights offer practical value for the design of scalable and high-precision indoor positioning systems.

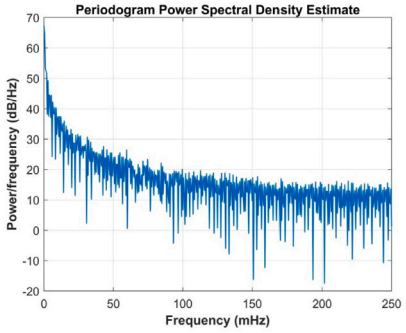


(a) IT002 beacon: estimated PSD at 1 m

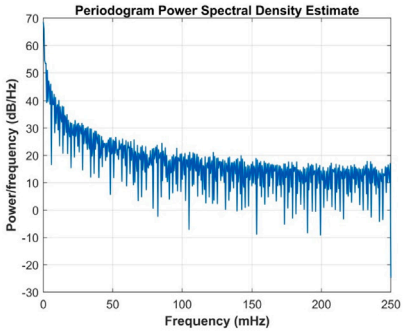
(b) IT008 beacon: estimated PSD at 1 m



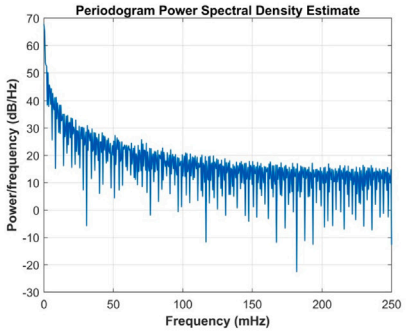
(c) IT002 beacon: estimated PSD at 3 m



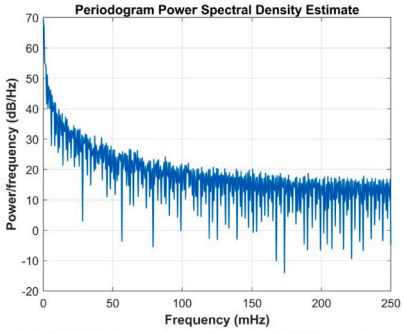
(d) IT008 beacon: estimated PSD at 3 m



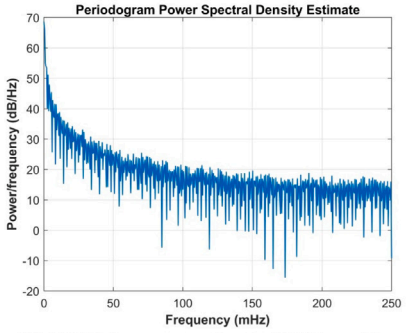
(e) IT002 beacon: estimated PSD at 5 m



(f) IT008 beacon: estimated PSD at 5 m



(g) IT002 beacon: estimated PSD at 10 m



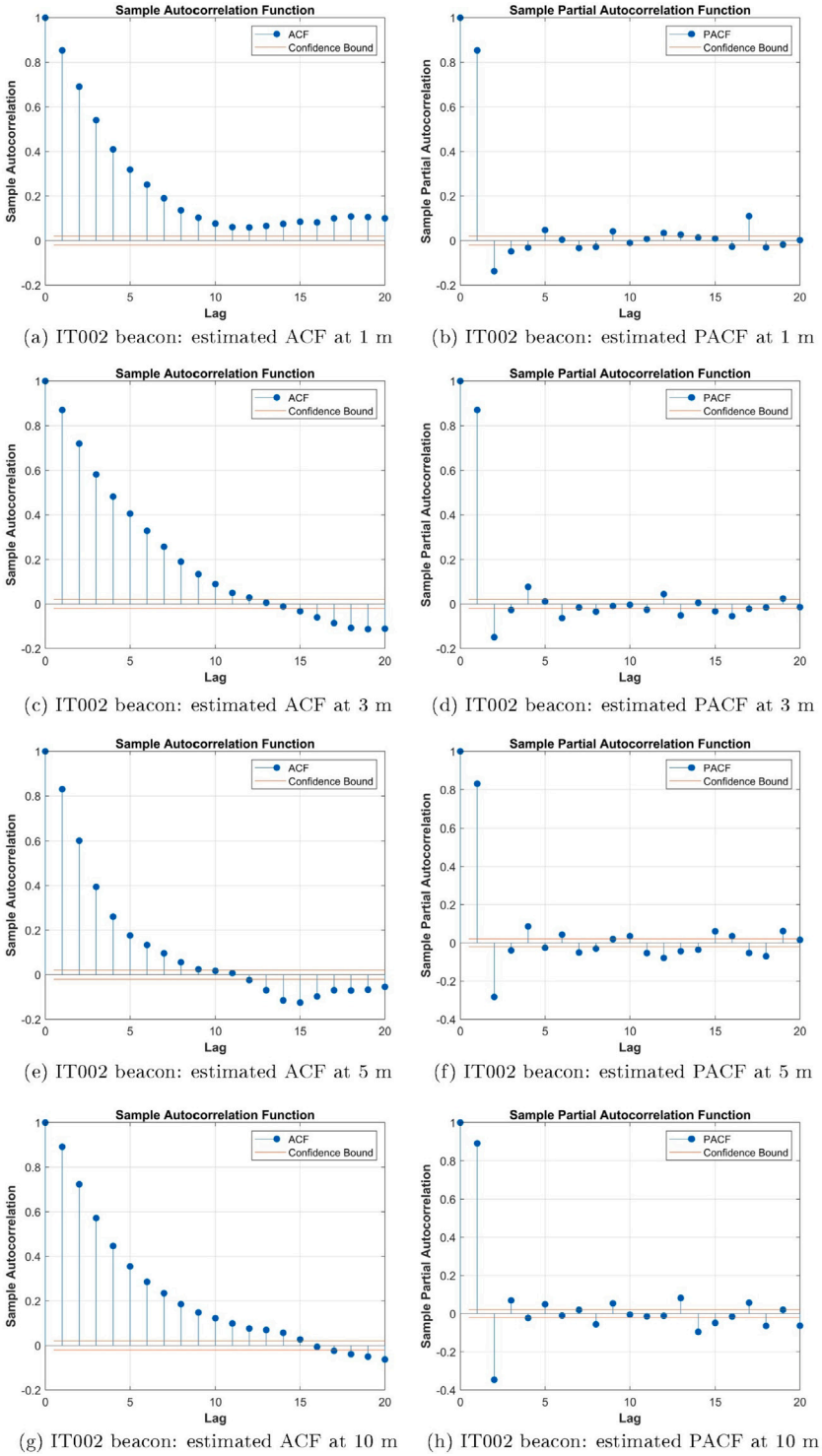
(h) IT008 beacon: estimated PSD at 10 m

Fig. 6. Estimated PSD of RSSI measurements for both beacons at distances of 1, 3, 5, and 10 m.

5. Conclusion and recommendations

This study presented a comprehensive stochastic–functional framework for the modeling of BLE RSSI measurements, with the objective of improving the estimation of RSSI–distance model parameters and enhancing the reliability of distance-based indoor positioning systems. The proposed methodology integrates stochastic covariance modeling and functional parameter estimation within a unified adjustment framework, thereby enabling the simultaneous characterization of temporal correlations, environmental effects, and beacon-specific transmission characteristics. Experiments were conducted using two BLE beacon types under controlled conditions to investigate their intrinsic signal behavior and to establish statistically rigorous RSSI–distance models.

The analysis revealed that BLE RSSI measurements exhibit significant temporal correlations that cannot be adequately represented by the commonly adopted white-noise assumption. Autocorrelation and partial autocorrelation analyses demonstrated that the RSSI noise is well characterized by a second-order autoregressive process, AR(2),



(a) IT002 beacon: estimated ACF at 1 m (b) IT002 beacon: estimated PACF at 1 m

(c) IT002 beacon: estimated ACF at 3 m (d) IT002 beacon: estimated PACF at 3 m

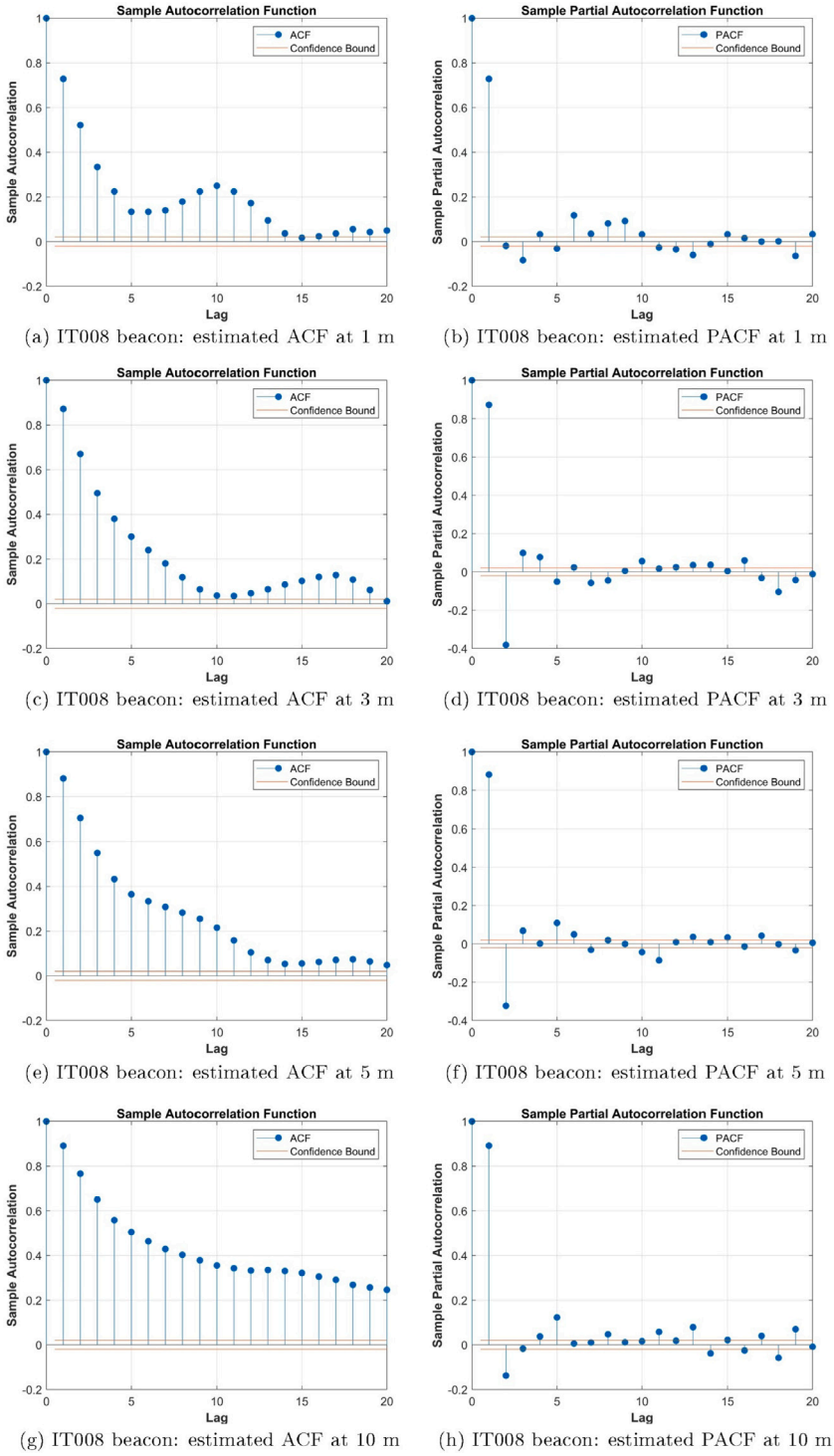
(e) IT002 beacon: estimated ACF at 5 m (f) IT002 beacon: estimated PACF at 5 m

(g) IT002 beacon: estimated ACF at 10 m (h) IT002 beacon: estimated PACF at 10 m

Fig. 7. Estimated ACF and PACF of RSSI measurements for the IT002 beacon at distances of 1, 3, 5, and 10 m.

under the considered experimental conditions. The stochastic properties were quantified through LS-VCE, while the functional parameters of the RSSI–distance model were estimated using the BLUE. The statistical consistency of the resulting model was subsequently verified using MLE, which identified the AR(2) model as the most appropriate stochastic representation among the candidate models considered.

The reconstructed RSSI signals achieved RMSE values of 1.12 dBm and 0.50 dBm for the IT002 and IT008 beacons, respectively, at a distance of 1 m, increasing to 2.19 dBm and 2.40 dBm at 10 m. These reconstruction accuracies correspond to relative distance uncertainties of approximately 6–13% at 1 m and 15–25% at 10 m, confirming the capability of the proposed framework to accurately characterize BLE signal behavior and support reliable RSSI-based ranging. The results further indicated that the temporal persistence of RSSI noise increases with distance, reflecting stronger multipath effects and emphasizing the importance of distance-dependent stochastic modeling and weighting strategies in positioning and sensor-fusion applications.



(a) IT008 beacon: estimated ACF at 1 m (b) IT008 beacon: estimated PACF at 1 m

(c) IT008 beacon: estimated ACF at 3 m (d) IT008 beacon: estimated PACF at 3 m

(e) IT008 beacon: estimated ACF at 5 m (f) IT008 beacon: estimated PACF at 5 m

(g) IT008 beacon: estimated ACF at 10 m (h) IT008 beacon: estimated PACF at 10 m

Fig. 8. Estimated ACF and PACF of RSSI measurements for the IT008 beacon at distances of 1, 3, 5, and 10 m.

The study also highlighted beacon-dependent differences in transmission characteristics, particularly with respect to maximum transmission power, demonstrating the importance of device-specific calibration. Although a common path-loss exponent was adopted in the present analysis, the proposed framework can be extended to accommodate beacon-specific propagation parameters in heterogeneous deployment scenarios.

Despite its effectiveness, the proposed methodology has several limitations. First, the experiments were conducted in a controlled, static outdoor environment to isolate signal behavior and accurately characterize the intrinsic stochastic properties of BLE RSSI measurements. While this controlled setup enabled rigorous estimation of both stochastic and functional model parameters, it also represents a limitation of the present study. In practical indoor positioning applications, signal propagation is affected by dynamic factors such as human movement, shadowing, environmental changes, and time-varying multipath conditions, which may introduce non-stationary behavior and more complex stochastic processes than those observed in the present experiments.

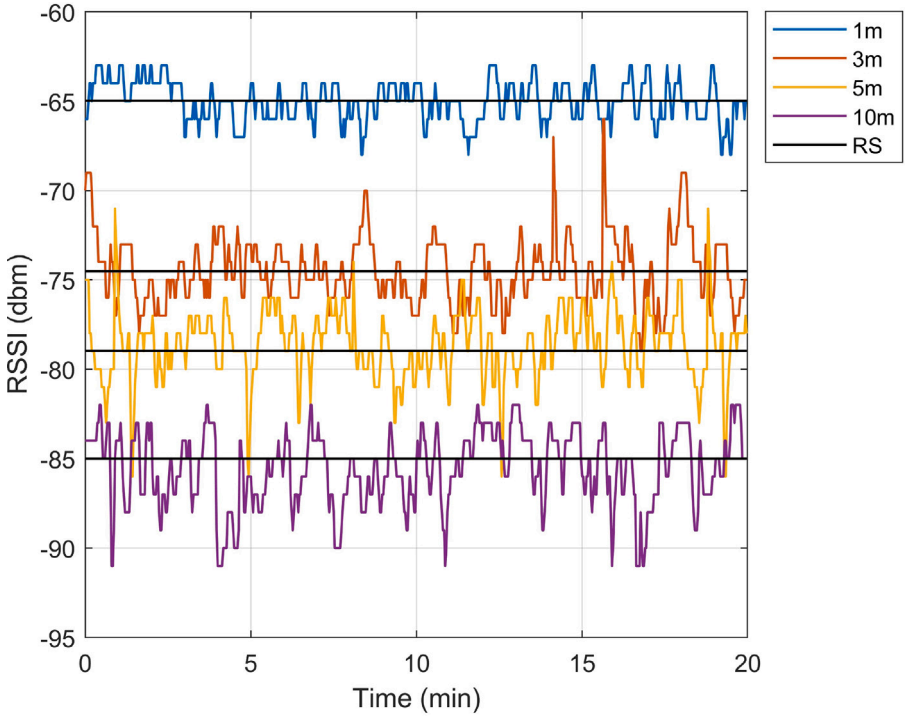


Fig. 9. All measurement and reconstructed signals of the IT002 beacon (denoted as 'RS') are provided by the stochastic and functional model.

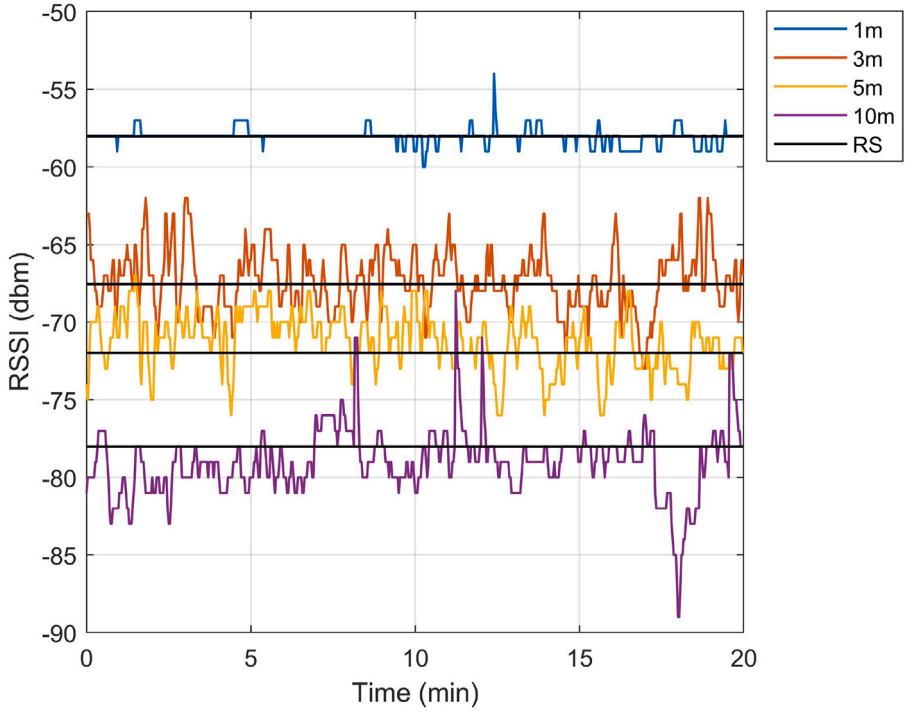


Fig. 10. All measurement and reconstructed signals of the IT008 beacon (denoted as 'RS') are provided by the stochastic and functional model.

Consequently, the model parameters estimated in this study should be regarded as calibration parameters that must be identified or updated prior to deployment in real-time dynamic positioning systems.

Another limitation is that the proposed framework is specifically developed for RSSI-based ranging and RSSI–distance model calibration. Although the methodology substantially improves distance estimation accuracy through the joint treatment of stochastic and functional characteristics, it is not directly applicable to Bluetooth AoA positioning, where localization is based on directional measurements rather than RSSI-derived distances. Therefore, the proposed approach primarily benefits distance-based BLE positioning systems and requires further adaptation for angle-based localization techniques.

Despite these limitations, the proposed framework establishes a statistically rigorous foundation for RSSI–distance modeling by explicitly accounting for temporal correlations, environmental variability, and measurement uncertainty. Future research should validate the

methodology in dynamic indoor environments involving human activity, shadowing, and varying channel conditions, investigate adaptive online estimation of stochastic and functional parameters for real-time positioning applications, and extend the framework to heterogeneous multi-beacon and multi-receiver configurations. Furthermore, given the increasing availability of Bluetooth 5.1 and later versions supporting AoA measurements, a promising direction is the integration of the proposed RSSI stochastic–functional modeling framework with AoA-based positioning to develop hybrid distance–angle localization systems capable of achieving improved robustness, reliability, and positioning accuracy.

In conclusion, this work presents a unified stochastic–functional framework for BLE RSSI modeling that combines covariance estimation through LS-VCE with functional parameter estimation using BLUE. The results demonstrate that RSSI noise exhibits significant temporal correlation and is best represented by an AR(2) process under the considered experimental conditions. By systematically modeling both the stochastic and functional characteristics of RSSI measurements, the proposed methodology provides statistically consistent parameter estimation and supports more reliable distance determination, thereby contributing to the theoretical development and practical implementation of high-precision BLE-based indoor positioning systems.

CRediT authorship contribution statement

Mohammad Mahdi Kariminejad: Writing – review & editing, Writing – original draft, Methodology, Investigation, Formal analysis, Data curation, Conceptualization. **Mohammad Ali Sharifi:** Writing – review & editing, Writing – original draft, Supervision, Conceptualization. **Alireza Amiri-Simkooei:** Writing – review & editing, Writing – original draft, Supervision, Methodology, Investigation, Conceptualization. **Mir Abolfazl Mostafavi:** Writing – review & editing, Supervision, Data curation, Conceptualization.

Declaration of competing interest

The authors declare no conflicts of interest. This manuscript has been approved by all authors, is original, has not been published previously, and is not under consideration elsewhere.

Acknowledgments

The authors thank the anonymous reviewers for their constructive comments, which improved the quality of this paper. OpenAI's ChatGPT was used to assist in preparing and refining the graphical abstract. All outputs were reviewed and modified by the authors, who take full responsibility for the final content.

Data availability

Data will be made available on request.

References

[1] G.K. Fischer, T. Schaechtle, A. Gabbrielli, J. Bordoy, I. Häring, F. Höflinger, S.J. Rupitsch, A systematic survey and comparative analysis of angular-based indoor localization and positioning technologies, IEEE Commun. Surv. Tutor. (2025) http://dx.doi.org/10.1109/comst.2025.3567765.

[2] B. Pinto, Y. Assayag, R. Barreto, H. Oliveira, Optimaps: A site survey-free indoor positioning system based on rssi diversity and sequential least squares programming, IEEE Internet Things J. (2025) http://dx.doi.org/10.1109/jiot.2025.3645666.

[3] X. Li, Y. Guo, F. Tan, L. He, Ble indoor localization method based on multidomain information fusion, IEEE Trans. Instrum. Meas. 75 (2025) 1–13, http://dx.doi.org/10.1109/tim.2025.3648000.

[4] W. Xue, W. Qiu, X. Hua, K. Yu, Improved wi–fi rssi measurement for indoor localization, IEEE Sens. J. 17 (2017) 2224–2230, http://dx.doi.org/10.1109/jsen.2017.2660522.

[5] O. Dhawahir, M. Torlak, Device-free wi-fi localization via deep learning on two-way csi, IEEE Access 14 (2026) 6747–6756, http://dx.doi.org/10.1109/access.2026.3651725.

[6] H. Guo, H. Li, J. Xiong, M. Yu, Indoor positioning system based on particle swarm optimization algorithm, Measurement 134 (2019) 908–913, http://dx.doi.org/10.1016/j.measurement.2018.12.038.

[7] C.-Y. Yao, W.-C. Hsia, An indoor positioning system based on the dual–channel passive rfid technology, IEEE Sens. J. 18 (2018) 4654–4663, http://dx.doi.org/10.1109/jsen.2018.2828044.

[8] Y. Zhou, W. Jiang, B. Cai, X. Hu, J. Wang, C. Deng, J. Liu, B. Li, A novel nlos correction approach for harsh indoor settings, IEEE Internet Things J. (2026) http://dx.doi.org/10.1109/jiot.2026.3658778.

[9] M. Ghaemifar, S. Motie, S.M. Moosaviun, Y. Nemati, S. Ebadollahi, Bluetooth low energy for indoor positioning: Challenges, algorithms and datasets, Autom. Constr. 177 (2025) 106316, http://dx.doi.org/10.1016/j.autcon.2025.106316.

[10] X. Chen, S. Zou, Improved wi–fi indoor positioning based on particle swarm optimization, IEEE Sens. J. 17 (2017) 7143–7148, http://dx.doi.org/10.1109/jsen.2017.2749762.

[11] T. Xiang, Y. Sun, G. Shen, Modefa: Multi-observer and denoising-enhanced fingerprint augmentation for semi-supervised wi-fi rss-based indoor positioning, IEEE Internet Things J. (2025) http://dx.doi.org/10.1109/jiot.2025.3573967.

[12] V. Bianchi, P. Ciampolini, I. De Munari, Rssi–based indoor localization and identification for zigbee wireless sensor networks in smart homes, IEEE Trans. Instrum. Meas. 68 (2018) 566–575, http://dx.doi.org/10.1109/tim.2018.2851675.

[13] J. Li, S. Yu, Z. Wei, Z. Zhou, An enhanced zigbee-based indoor localization method using multi-stage rssi filtering and lqi-aware mle, Sensors 25 (2025) 2947, http://dx.doi.org/10.3390/s25092947.

[14] J.S. Pereira, Long-range rfid indoor positioning system for an autonomous wheelchair, Sensors 25 (2025) 2542, http://dx.doi.org/10.3390/s25082542.

[15] Y.-F. Huang, T.-J. Chan, G.-Y. Chen, H.-W. Wang, An improved particle swarm optimization for three-dimensional indoor positioning with ultra-wideband communications for los/nlos channels, Mathematics 14 (2026) 493, http://dx.doi.org/10.3390/math14030493.

[16] L. Cheng, Z. Fu, An adaptive kalman filter loosely coupled indoor fusion positioning system based on inertial navigation system and ultra-wide band, Measurement 244 (2025) 116412, http://dx.doi.org/10.1016/j.measurement.2024.116412.

[17] M.M. Kariminejad, M.A. Mostafavi, M.A. Sharifi, A. Amiri-Simkooei, Location-based services in complex indoor environments via modern smartphone multi-sensor integrated navigation, Abstr. ICA 10 (2025) 139, http://dx.doi.org/10.5194/ica-abs-10-139-2025.

[18] M.M. Kariminejad, M.A. Sharifi, A. Amiri-Simkooei, M.A. Mostafavi, Impact of model uncertainty and sensor deployment geometry on the precision of BLE RSSI-based indoor positioning, IEEE Sens. J. 26 (2025) 2181–2193, http://dx.doi.org/10.1109/jsen.2025.3637898.

[19] T.-M.T. Dinh, N.-S. Duong, K. Sandrasegaran, Smartphone–based indoor positioning using ble ibeacon and reliable lightweight fingerprint map, IEEE Sens. J. 20 (2020) 10283–10294, http://dx.doi.org/10.1109/jsen.2020.2989411.

[20] W. Wu, D. Zhou, L. Shen, Z. Zhao, C. Li, G. Huang, Transaoa: Transformer–based angle of arrival estimation for ble indoor localization, IEEE Trans. Instrum. Meas. (2025) http://dx.doi.org/10.1109/tim.2025.3529535.

[21] G. Li, E. Geng, Z. Ye, Y. Xu, J. Lin, Y. Pang, Indoor positioning algorithm based on the improved rssi distance model, Sensors 18 (2018) 2820, http://dx.doi.org/10.3390/s18092820.

[22] A.M. Hossain, W.-S. Soh, A comprehensive study of bluetooth signal parameters for localization, in: 2007 IEEE 18th International Symposium on Personal, Indoor and Mobile Radio Communications, IEEE, 2007, pp. 1–5, http://dx.doi.org/10.1109/pimrc.2007.4394215.

[23] L. Pei, R. Chen, J. Liu, T. Tenhunen, H. Kuusniemi, Y. Chen, Inquiry–based bluetooth indoor positioning via rssi probability distributions, in: 2010 Second International Conference on Advances in Satellite and Space Communications, IEEE, 2010, pp. 151–156, http://dx.doi.org/10.1109/spacomm.2010.18.

[24] F. Subhan, H. Hasbullah, A. Rozyyev, S.T. Bakhsh, Indoor positioning in bluetooth networks using fingerprinting and lateration approach, in: 2011 International Conference on Information Science and Applications, IEEE, 2011, pp. 1–9, http://dx.doi.org/10.1109/icisa.2011.5772436.

[25] S. Kajioka, T. Mori, T. Uchiya, I. Takumi, H. Matsuo, Experiment of indoor position presumption based on rssi of bluetooth le beacon, in: 2014 IEEE 3rd Global Conference on Consumer Electronics, GCCE, IEEE, 2014, pp. 337–339, http://dx.doi.org/10.1109/gcce.2014.7031308.

[26] M. Ji, J. Kim, J. Jeon, Y. Cho, Analysis of positioning accuracy corresponding to the number of ble beacons in indoor positioning system, in: 2015 17th International Conference on Advanced Communication Technology, ICACT, IEEE, 2015, pp. 92–95, http://dx.doi.org/10.1109/icact.2015.7224764.

[27] A. Thaljaoui, T. Val, N. Nasri, D. Brulin, Ble localization using rssi measurements and iringla, in: 2015 IEEE International Conference on Industrial Technology, ICIT, IEEE, 2015, pp. 2178–2183, http://dx.doi.org/10.1109/icit.2015.7125418.

[28] M. Altini, D. Brunelli, E. Farella, L. Benini, Bluetooth indoor localization with multiple neural networks, in: IEEE 5th International Symposium on Wireless Pervasive Computing 2010, IEEE, 2010, pp. 295–300, http://dx.doi.org/10.1109/iswpc.2010.5483748.

[29] F. Zafari, I. Papapanagiotou, Enhancing ibeacon based micro–location with particle filtering, in: 2015 IEEE Global Communications Conference, GLOBECOM, IEEE, 2015, pp. 1–7, http://dx.doi.org/10.1109/glocom.2015.7417504.
[30] S. Chai, R. An, Z. Du, An indoor positioning algorithm using bluetooth low energy rssi, in: 2016 International Conference on Advanced Materials Science and Environmental Engineering, Atlantis Press, 2016, pp. 274–276, http://dx.doi.org/10.2991/amsee-16.2016.72.
[31] X. Li, D. Xu, X. Wang, R. Muhammad, Design and implementation of indoor positioning system based on ibeacon, in: 2016 International Conference on Audio, Language and Image Processing, ICALIP, IEEE, 2016, pp. 126–130, http://dx.doi.org/10.1109/icalip.2016.7846648.
[32] Y. Peng, W. Fan, X. Dong, X. Zhang, An iterative weighted knn (iw–knn) based indoor localization method in bluetooth low energy (ble) environment, in: 2016 Intl IEEE Conferences on Ubiquitous Intelligence & Computing, Advanced and Trusted Computing, Scalable Computing and Communications, Cloud and Big Data Computing, Internet of People, and Smart World Congress (UIC/ATC/ScalCom/CBDCom/IoP/SmartWorld), IEEE, 2016, pp. 794–800, http://dx.doi.org/10.1109/uic-atc-scalcom-cbdcom-iop-smartworld.2016.0127.
[33] Z. Zuo, L. Liu, L. Zhang, Y. Fang, Indoor positioning based on bluetooth low–energy beacons adopting graph optimization, Sensors 18 (2018) 3736, http://dx.doi.org/10.3390/s18113736.
[34] Y. Wang, X. Yang, Y. Zhao, Y. Liu, L. Cuthbert, Bluetooth positioning using rssi and triangulation methods, in: 2013 IEEE 10th Consumer Communications and Networking Conference, CCNC, IEEE, 2013, pp. 837–842, http://dx.doi.org/10.1109/ccnc.2013.6488558.
[35] C. Zhou, J. Yuan, H. Liu, J. Qiu, Bluetooth indoor positioning based on rssi and kalman filter, Wirel. Pers. Commun. 96 (2017) 4115–4130, http://dx.doi.org/10.1007/s11277-017-4371-4.
[36] X. Hou, T. Arslan, J. Gu, Indoor localization for bluetooth low energy using wavelet and smoothing filter, in: 2017 International Conference on Localization and GNSS, (ICL–GNSS), IEEE, 2017, pp. 1–6, http://dx.doi.org/10.1109/icl-gnss.2017.8376247.
[37] R. Ramirez, C.-Y. Huang, C.-A. Liao, P.-T. Lin, H.-W. Lin, S.-H. Liang, A practice of ble rssi measurement for indoor positioning, Sensors 21 (2021) 5181, http://dx.doi.org/10.3390/s21155181.
[38] N. Yu, X. Zhan, S. Zhao, Y. Wu, R. Feng, A precise dead reckoning algorithm based on bluetooth and multiple sensors, IEEE Internet Things J. 5 (2017) 336–351, http://dx.doi.org/10.1109/jiot.2017.2784386.
[39] Y. Zhuang, J. Yang, Y. Li, L. Qi, N. El-Sheimy, Smartphone–based indoor localization with bluetooth low energy beacons, Sensors 16 (2016) 596, http://dx.doi.org/10.3390/s16050596.
[40] Y. Liu, C. Wu, X. Kong, X. Du, Y. You, A tightly–coupled method for indoor vehicle navigation based on smartphone imu and ble, IEEE Trans. Instrum. Meas. (2024) http://dx.doi.org/10.1109/tim.2024.3481552.
[41] P. Sthapit, H.-S. Gang, J.-Y. Pyun, Bluetooth based indoor positioning using machine learning algorithms, in: 2018 IEEE International Conference on Consumer Electronics–Asia, (ICCE–Asia), IEEE, 2018, pp. 206–212, http://dx.doi.org/10.1109/icce-asia.2018.8552138.
[42] K. Huang, K. He, X. Du, A hybrid method to improve the ble–based indoor positioning in a dense bluetooth environment, Sensors 19 (2019) 424, http://dx.doi.org/10.3390/s19020424.
[43] L. Bai, F. Ciravegna, R. Bond, M. Mulvenna, A low cost indoor positioning system using bluetooth low energy, IEEE Access 8 (2020) 136858–136871, http://dx.doi.org/10.1109/access.2020.3012342.
[44] A. Afghantoloee, M.A. Mostafavi, A purpose–oriented 3d voronoi algorithm for deployment of a multi–type sensor network in complex 3d indoor environments in support of the mobility of people with motor disabilities, IEEE Trans. Instrum. Meas. (2024) http://dx.doi.org/10.1109/tim.2024.3398087.
[45] Y. Assayag, H. Oliveira, E. Souto, R. Barreto, R. Pazzi, A model–based ble indoor positioning system using particle swarm optimization, IEEE Sens. J. 24 (2024) 6898–6908, http://dx.doi.org/10.1109/jsen.2024.3352535.
[46] P. Bencak, D. Hercog, T. Lerher, Indoor positioning system based on bluetooth low energy technology and a nature–inspired optimization algorithm, Electronics 11 (2022) 308, http://dx.doi.org/10.3390/electronics11030308.
[47] A. Koutris, T. Siozos, Y. Kopsinis, A. Pikrakis, T. Merk, M. Mahlig, S. Papaharalabos, P. Karlsson, Deep learning–based indoor localization using multi–view ble signal, Sensors 22 (2022) 2759, http://dx.doi.org/10.3390/s22072759.
[48] S. Monfared, T.-H. Nguyen, L. Petrillo, P. De Doncker, F. Horlin, Experimental demonstration of ble transmitter positioning based on aoa estimation, in: 2018 IEEE 29th Annual International Symposium on Personal, Indoor and Mobile Radio Communications, PIMRC, IEEE, 2018, pp. 856–859, http://dx.doi.org/10.1109/pimrc.2018.8580796.
[49] Q. Wan, T. Wu, K. Zhang, X. Liu, K. Cheng, J. Liu, J. Zhu, A high precision indoor positioning system of ble aoa based on isss algorithm, Measurement 224 (2024) 113801, http://dx.doi.org/10.1016/j.measurement.2023.113801.
[50] B. Shin, J.H. Lee, T. Lee, Novel indoor fingerprinting method based on rss sequence matching, Measurement 223 (2023) 113719, http://dx.doi.org/10.1016/j.measurement.2023.113719.
[51] F.C. Marchi, A.L.S. Gradvohl, Studies on indoor positioning algorithms using ble beacons, Rev. Bras. Comput. Apl. 15 (2023) 106–114, http://dx.doi.org/10.5335/rbca.v15i3.14592.
[52] A. Fabris, O.K. Rayel, J.L. Rebelatto, G.L. Moritz, R.D. Souza, Aoa and rssi–based ble indoor positioning system with kalman filter and data fusion, IEEE Internet Things J. (2025) http://dx.doi.org/10.1109/jiot.2025.3530866.
[53] C. Yang, Load-dependent structural state reconstruction-oriented and reliability-based sensor placement optimization method, AIAA J. (2025) 1–12, http://dx.doi.org/10.2514/1.j065285.
[54] H. Gao, X. Liu, Y. Bi, C. Yang, Fixed-time safety-critical attitude control for flexible spacecraft with actuator faults, Acta Astronaut. (2025) http://dx.doi.org/10.1016/j.actaastro.2025.09.097.
[55] J. Röbesaat, P. Zhang, M. Abdelaal, O. Theel, An improved ble indoor localization with kalman–based fusion: An experimental study, Sensors 17 (2017) 951, http://dx.doi.org/10.3390/s17050951.
[56] H. Chen, H. Wang, T. Dong, J. Song, A mlp-bigru model based dynamic displacement estimation method for multi state indoor positioning, IEEE Trans. Instrum. Meas. (2026) http://dx.doi.org/10.1109/tim.2026.3654740.
[57] X. Hou, T. Arslan, Monte carlo localization algorithm for indoor positioning using bluetooth low energy devices, in: 2017 International Conference on Localization and GNSS, (ICL–GNSS), IEEE, 2017, pp. 1–6, http://dx.doi.org/10.1109/icl-gnss.2017.8376248.
[58] G. Wei, X. Luo, H. Yang, S. Du, F. Liu, Shsloc: Semi-hard sample calibration and bclpso for indoor localization, IEEE Trans. Veh. Technol. (2026) http://dx.doi.org/10.1109/tvt.2026.3659491.
[59] Q. Yu, C. Yang, G. Dai, L. Peng, Non-probabilistic set-based selection strategy for multi-objective optimization with interval uncertainties, Swarm Evol. Comput. 98 (2025) 102153, http://dx.doi.org/10.1016/j.swevo.2025.102153.
[60] W. Lu, C. Yang, Y. Xia, Compliant predictive tracking control of space manipulator under safety assessment, IEEE Trans. Aerosp. Electron. Syst. (2025) http://dx.doi.org/10.1109/taes.2025.3649476.
[61] Y. You, C. Wu, Hybrid indoor positioning system for pedestrians with swinging arms based on smartphone imu and rssi of ble, IEEE Trans. Instrum. Meas. 70 (2021) 1–15, http://dx.doi.org/10.1109/tim.2021.3084286.
[62] X. Kong, C. Wu, Y. You, Y. Yuan, Hybrid indoor positioning method of ble and pdr based on adaptive feedback ekf with low ble deployment density, IEEE Trans. Instrum. Meas. 72 (2022) 1–12, http://dx.doi.org/10.1109/tim.2022.3227957.
[63] X. Kong, C. Wu, Y. You, Z. Lv, Z. Zhao, Hybrid indoor positioning method of ble and monocular vins–based smartphone, IEEE Trans. Instrum. Meas. 72 (2023) 1–13, http://dx.doi.org/10.1109/tim.2023.3295010.
[64] A.M. Pessoa, I.M. Guerreiro, C.F. e Silva, F.R. Cavalcanti, A positive semidefinite autocorrelation function for modeling 3d gaussian processes, IEEE Trans. Veh. Technol. 70 (2021) 1941–1945, http://dx.doi.org/10.1109/tvt.2021.3055040.
[65] G. Ali, F. Mohd-Yasin, Arima modeling of noise of piezoelectric accelerometer, IEEE Access (2025) http://dx.doi.org/10.1109/access.2025.3581427.
[66] P.J. Teunissen, A. Amiri-Simkooei, Least–squares variance component estimation, J. Geod. 82 (2008) 65–82, http://dx.doi.org/10.1007/s00190-007-0157-x.
[67] A. Amiri-Simkooei, Least-Squares Variance Component Estimation: Theory and GPS Applications (Ph.D. thesis), Delft University of Technology, Publication on Geodesy, 64, Netherlands Geodetic Commission, 2007.
[68] A. Amiri-Simkooei, C. Tiberius, Assessing receiver noise using GPS short baseline time series, GPS Solutions 11 (2007) 21–35, http://dx.doi.org/10.1007/s10291-006-0026-8.
[69] A. Amiri-Simkooei, C.C.J.M. Tiberius, P.J.G. Teunissen, Assessment of noise in GPS coordinate time series: methodology and results, J. Geophys. Res. 112 (2007) B07413, http://dx.doi.org/10.1029/2006JB004913.
[70] M.R. Toribio, A.G. Menéndez, S.R. Toribio, I.A. García, A novel approach to speed up hampel filter for outlier detection, Sensors (2025) http://dx.doi.org/10.3390/s25113319.
[71] G.E. Box, G.M. Jenkins, G.C. Reinsel, G.M. Ljung, Time series analysis: forecasting and control, John Wiley & Sons, 2015, http://dx.doi.org/10.1057/9781137291264_6.
[72] A. Dürre, R. Fried, T. Liboschik, Robust estimation of (partial) autocorrelation, Wiley Interdiscip. Rev.: Comput. Stat. 7 (2015) 205–222, http://dx.doi.org/10.1002/wics.1351.
[73] X. Ding, Z. Zhou, On the partial autocorrelation function for locally stationary time series: characterization, estimation and inference, Biometrika 112 (2025) asaf016, http://dx.doi.org/10.1093/biomet/asaf016.
[74] R. Killick, M.I. Knight, G.P. Nason, I.A. Eckley, The local partial autocorrelation function and some applications, 2020, http://dx.doi.org/10.1214/20-ejs1748.
[75] S. Chiang, J. Zito, V.R. Rao, M. Vannucci, Time-series analysis, in: Statistical Methods in Epilepsy, Chapman and Hall/CRC, 2024, pp. 166–200, http://dx.doi.org/10.1201/9781003254515-8.
[76] S. Shirafkan, M.A. Sharifi, S. Belda, S.M. Khazraei, A. Amiri-Simkooei, S. Modiri, Analysis of periodic patterns, noise characteristics, and predictive modeling of polar motion and length of day, Adv. Space Res. (2025) http://dx.doi.org/10.1016/j.asr.2025.05.090.
[77] A. Amiri-Simkooei, Noise in multivariate GPS position time-series, J. Geod. 83 (2009) 175–187, http://dx.doi.org/10.1007/s00190-008-0251-8.
[78] A.R. Amiri-Simkooei, T.H. Mohammadloo, D.F. Argus, Multivariate analysis of GPS position time series of JPL second reprocessing campaign, J. Geod. 91 (2017) 685–704, http://dx.doi.org/10.1007/s00190-016-0991-9.
[79] P.J. Teunissen, Adjustment Theory: An Introduction, TU Delft OPEN Publishing, 2024, http://dx.doi.org/10.59490/tb.95.